Inorg. Chem. **2007**, *46*, 6299–6310

Copper(II), Cobalt(II), and Nickel(II) Complexes with a Bulky Anthracene-Based Carboxylic Ligand: Syntheses, Crystal Structures, and Magnetic Properties

Chun-Sen Liu,[†] Jun-Jie Wang,[†] Li-Fen Yan,[†] Ze Chang,[†] Xian-He Bu,*[,†] E. Carolina Sañudo,[‡] and Joan Ribas[‡]

Department of Chemistry, Nankai University, Tianjin 300071, People's Republic of China, and Departament de Química Inorgànica, Universitat de Barcelona, Diagonal 647, 08028-Barcelona, Spain

Received January 17, 2007

To systematically explore the influence of the bulky aromatic ring skeleton with a large conjugated π-system on the structures and properties of their complexes, six Cu^{II}, Co^{II}, and Ni^{II} complexes with the anthracene-based carboxylic ligand anthracene-9-carboxylic acid (H**L**^{1}), were synthesized and characterized, sometimes incorporating different auxiliary ligands: $[Cu_2(\mathbf{L}^1)_4(CH_3OH)_2](CH_3OH)$ (**1**), $[Cu_4(\mathbf{L}^1)_6(\mathbf{L}^2)_4](NO_3)_2(H_2O)_2$ (**2**), $\{[Cu_2(\mathbf{L}^1)_4(\mathbf{L}^3)](CH_3OH)_{0.25}\}_\infty$ (**3**), $[Co_2(\mathbf{L}^1)_4(\mathbf{L}^4)_2(\mu\text{-}H_2O)](CH_3OH)$ (**4**), $\{[Co(\mathbf{L}^1)_2(\mathbf{L}^5)(CH_3OH)_2]\}_\infty$ (**5**), and $\{[Ni(\mathbf{L}^1)_2(\mathbf{L}^5)(CH_3OH)_2]\}_\infty$ (**6**) (**L**^{2} = 2,2′-bipyridine, **L**^{3} = 1,4-diazabicyclo[2.2.2]octane, **L**^{4} = 1,10-phenanthroline, and **L**^{5} = 4,4′-bipyridine). **1** has a dinuclear structure that is further assembled to form a one-dimensional (1D) chain and then a two-dimensional (2D) network by the C–H···O H-bonding and $\pi\cdots\pi$ stacking interactions jointly. **2** takes a tetranuclear structure due to the existence of the chelating **L**^{2} ligand. **3** possesses a 1D chain structure by incorporating the related auxiliary ligand **L**^{3}, which is further interlinked via interchain $\pi\cdots\pi$ stacking, resulting in a three-dimensional (3D) network. **4** also has a dinuclear structure and then forms a higher-dimensional supramolecular network through intermolecular $\pi\cdots\pi$ stacking and/or C–H$\cdots\pi$ interactions. **5** and **6** are isostructural complexes, except they involve different metal ions, showing 1D chain structures, which are also assembled into 2D networks from the different crystallographic directions by interchain $\pi\cdots\pi$ stacking and C–H$\cdots\pi$ interactions, respectively. The results reveal that the steric bulk of the anthracene ring in H**L**^{1} plays an important role in the formation of **1**–**6**. The magnetic properties of the complexes were investigated, and the very long intermetallic distances result in weak magnetic coupling, with the exception of **1** and **3**, which adopt the typical paddle-wheel structure of copper acetate and are thus strongly coupled.

Introduction

In recent years, the rational design and synthesis of functional coordination architectures has attracted great interest because of not only their interesting topologies but also their potential uses as functional materials.[1−2] The effective and facile approach for the synthesis of such complexes is still the appropriate choice of well-designed organic ligands as bridges or terminal groups (building blocks) with metal ions or metal clusters as nodes, which, so far, has been at an evolutionary stage with the current focus mainly on understanding the factors to determine the crystal packing.[1k,2,3] Among various ligands, the versatile carboxylic acid ligands exhibiting diverse coordination modes, especially for benzene-based and naphthalene-based carboxylic acids, such as 1,4-benzenedicarboxylic acid (**BDCA**),[4−6] 1,4-naphthalenedicarboxylic acid (**NDCA**),[7]

* To whom correspondence should be addressed. Fax: +86-22-23502458. E-mail: buxh@nankai.edu.cn.
[†] Nankai University.
[‡] Universitat de Barcelona.

(1) (a) Lehn, J.-M. *Supramolecular Chemistry*; VCH: Weinheim, Germany, 1995. (b) Stang, P. J.; Zhdankin, V. V. *Chem. Rev.* **1996**, *96*, 1123. (c) Yam, V. W. W.; Lo, K. K.-W.; Fung, W. K.-M.; Wang, C.-R. *Coord. Chem. Rev.* **1998**, *171*, 17. (d) Chen, C. H.; Shi, J. M. *Coord. Chem. Rev.* **1998**, *171*, 161. (e) Leininger, S.; Olenyuk, B.; Stang, P. J. *Chem. Rev.* **2000**, *100*, 853. (f) Moulton, B.; Zaworotko, M. J. *Chem. Rev.* **2001**, *101*, 1629. (g) Wang, S. *Coord. Chem. Rev.* **2001**, *215*, 79. (h) Evans, O. R.; Lin, W. *Acc. Chem. Res.* **2002**, *35*, 511. (i) Gade, L. H. *Acc. Chem. Res.* **2002**, *35*, 575. (j) Steel, P. J. *Acc. Chem. Res.* **2005**, *38*, 243. (k) Ye, B.-H.; Tong, M.-L.; Chen, X.-M. *Coord. Chem. Rev.* **2005**, *249*, 545. (l) Khlobystov, A. N.; Blake, A. J.; Champness, N. R.; Lemenovskii, D. A.; Majouga, A. G.; Zyk, N. V.; Schröder, M. *Coord. Chem. Rev.* **2001**, *222*, 155.

10.1021/ic070086y CCC: $37.00
Published on Web 07/04/2007

benzoic acid (H**BA**),[8] and 1-naphthalenecarboxylic acid (H**NCA**),[9a,b] have been well used in the preparations of various metal−organic complexes. For instance, a series of aromatic 1,4-benzenedicarboxylic-bridged Cu^{II},[4] Co^{II},[5] and Ni^{II} [6] metal−organic complexes with various functions have been well-documented by other groups.[4−6]

In comparison with the benzene-based and naphthalene-based carboxylic acid ligands aforementioned, however, far less common has been the investigation of anthracene-based carboxylic acids, such as anthracene-9-carboxylic acid[9a,b] (H$\mathbf{L^1}$) (see Chart 1). Similar to what we have found previously,[9] H$\mathbf{L^1}$ ligands bearing the bulky anthracene skeleton have two obvious characteristics: (1) they have larger conjugated π-systems, and therefore, $\pi\cdots\pi$ stacking and/or C−H$\cdots\pi$ interactions may play important roles in the formation of their complexes, especially in the aspect of linking the multinuclear discrete subunits or low-dimensional entities into higher-dimensional supramolecular frameworks; (2) the steric hindrance of the bulky anthracene ring may

Chart 1

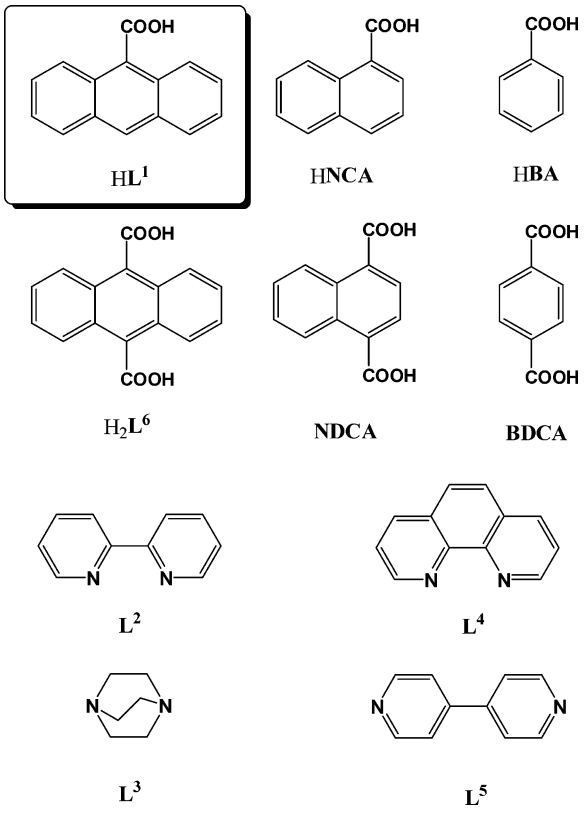

(2) For examples, see: (a) Fujita, M.; Kwon, Y. J.; Washizu, S.; Ogura, K. *J. Am. Chem. Soc.* **1997**, *116*, 1151. (b) Wong, W.-K.; Zhang, L.; Wong, W.-T. *Chem. Commun.* **1998**, 673. (c) Su, W.; Hong, M.; Weng, J.; Cao, R.; Lu, S. *Angew. Chem., Int. Ed.* **2000**, *39*, 2911. (d) Wang, Q.-M.; Mak, T. C. W. *J. Am. Chem. Soc.* **2001**, *123*, 7594. (e) Mao, Z.; Chao, H.-Y.; Hui, Z.; Che, C.-M.; Fu, W.-F.; Cheung, K.-K.; Zhu, N. *Chem.−Eur. J.* **2003**, *9*, 2885. (f) Wu, J.; Song, Y.; Zhang, E.; Hou, H.; Fan, Y.; Zhu, Y. *Chem.−Eur. J.* **2006**, *12*, 5823. (g) Hou, H.; Wei, Y.; Song, Y.; Mi, L.; Tang, M.; Li, L.; Fan, Y. *Angew. Chem., Int. Ed.* **2005**, *44*, 6067. (h) Chi, Y.-N.; Huang, K.-L.; Cui, F.- Y.;Xu, Y.-Q.; Hu, C.-W. *Inorg. Chem.* **2006**, *45*, 10605. (i) Gudbjartson, H.; Biradha, K.; Poirier, K. M.; Zaworotko, M. J. *J. Am. Chem. Soc.* **1999**, *121*, 2599. (j) Campos-Fern'andez, C. S.; Schottel, B. L.; Chifotides, H. T.; Bera, J. K.; Bacsa, J.; Koomen, J. M.; Russell, D. H.; Dunbar, K. R. *J. Am. Chem. Soc.* **2006**, *127*, 12909.

(3) For examples, see: (a) Jung, O.-S.; Kim, Y. J.; Lee, Y.-A.; Chae, H. K.; Jang, H. G.; Hong, J. *Inorg. Chem.* **2001**, *40*, 2105. (b) Steel, P. J. *Acc. Chem. Res.* **2005**, *38*, 243. (c) Han, Z.-B.; Cheng, X.-N.; Chen, X.- M. *Cryst. Growth Des.* **2005**, *5*, 695. (d) Liu, C.-S.; Chen, P.-Q.; Yang, E.-C.; Tian, J.-L.; Bu, X.-H.; Li, Z.-M.; Sun, H.-W.; Lin, Z. *Inorg. Chem.* **2006**, *45*, 5812. (e) Tong, L. H.; Li, J. R.; Liu, C. S.; Shi, X. S.; Zhou, J. N.; Bu, X. H.; Ribas, J. *Inorg. Chem.* **2006**, *45*, 162. (f) Li, D.; Wu, T. *Inorg. Chem.* **2005**, *44*, 1175. (g) Dong, Y.-B.; Wang, H.-Y.; Ma, J.-P.; Shen, D.-Z.; Huang, R.-Q. *Inorg. Chem.* **2005**, *44*, 4679.

(4) (a) Zhang, X.-M.; Tong, M.-L.; Chen, X.-M. *Angew. Chem., Int. Ed.* **2002**, *41*, 1029. (b) Kirillov, M.; Kopylovich, M. N.; Kirillova, M. V.; Haukka, M.; Guedes da Silva, M. F. C.; Pombeiro, A. J. L. *Angew. Chem., Int. Ed.* **2005**, *44*, 4345. (c) Du, M.; Jiang, X.-J.; Zhao, X.-J. *Chem. Commun.* **2005**, 5521. (d) Ohmura, T.; Mori, W.; Hasegawa, M.; Takei, T.; Yoshizawa, A. *Chem. Lett.* **2003**, *32*, 34. (e) Ma, A.-Q.; Shi, Z.; Xu, R.-R.; Pang, W.-Q.; Zhu, L.-G. *Chem. Lett.* **2003**, *32*, 1010. (f) Li, X.-H.; Yang, S.- Z.; Xiao, H.-P. *Cryst. Growth Des.* **2006**, *6*, 2392. (g) Mukherjee, P. S.; Ghoshal, D.; Zangrando, E.; Mallah, T.; Chaudhuri, N. R. *Eur. J. Inorg. Chem.* **2004**, 4675. (h) Hu, T.-L.; Li, J.-R.; Liu, C.-S.; Shi, X.-S.; Zhou, J.- N.; Bu, X.-H.; Ribas, J. *Inorg. Chem.* **2006**, *45*, 162. (i) Company, A.; G'omez, L.; Valbuena, J. M. L. Mas-Ballest'e, R.; Benet-Buchholz, J.; Llobet, A.; Costas. M. *Inorg. Chem.* **2006**, *45*, 2501. (j) Baeg, J. Y.; Lee, S. W. *Inorg. Chem. Commun.* **2003**, *6*, 313. (k) Bian, H.-D.; Xu, J.-Y.; Gu, W.; Yan, S.- P.; Liao, D.- Z.; Jiang, Z.- H.; Cheng, P. *Inorg. Chem. Commun.* **2003**, *6*, 573. (l) Zhu, L.-G.; Xiao, H.- P.; Lu, J. Y. *Inorg. Chem. Commun.* **2004**, *7*, 94. (m) Ray, A.; Mijanuddin, M.; Chatterjee, R.; Marek, J.; Mondal, S.; Ali, M. *Inorg. Chem. Commun.* **2006**, *9*, 167. (n) Zhang, Q.; Lu, C. *J. Chem. Crystallogr.* **2005**, *35*, 965. (o) Lin, D.-D.; Xu, D.-J. *J. Coord. Chem.* **2005**, *58*, 605.

(5) (a) Huang, Z.-L.; Drillon, M.; Masciocchi, N.; Sironi, A.; Zhao, J.-T.; Rabu, P.; Panissod, P. *Chem. Mater.* **2000**, *12*, 2805. (b) Fu, Z.-Y.; Wu, X.-T.; Dai, J.-C.; Hu, S.-M.; Du, W.-X.; Zhang, H.-H.; Sun, R.-Q. *Eur. J. Inorg. Chem.* **2002**, 2730. (c) Kurmoo, M.; Kumagai, H.; Green, M. A.; Lovett, B. W.; Blundell, S. J.; Ardavan, A.; Singleton, J. *J. Solid State Chem.* **2001**, *159*, 343. (d) Rosi, N. L.; Kim, J.; Eddaoudi, M.; Chen, B.; O Keeffe, M.; Yaghi, O. M. *J. Am. Chem. Soc.* **2005**, *127*, 1504. (e) Sun, D.; Cao, R.; Liang, Y.; Shi, Q.; Su, W.; Hong, M. *J. Chem. Soc., Dalton Trans.* **2001**, 2335. (f) Niu, S. Y.; Jin, J.; Yang, Z. Z. *Synth. React. Inorg. Met.-Org. Chem.* **2004**, *34*, 173. (g) Rabu, P.; Huang, Z.-L.; Hornick, C.; Drillon, M. *Synth. Met.* **2001**, *122*, 509.

(6) (a) Groeneman, R. H.; MacGillivray, L. R.; Atwood, J. L. *Inorg. Chem.* **1999**, *38*, 208. (b) Go, Y. B.; Wang, X.; Anokhina, E. V.; Jacobson, A. J. *Inorg. Chem.* **2004**, *43*, 5360. (c) Go, Y. B.; Wang, X.; Anokhina, E. V.; Jacobson, A. J. *Inorg. Chem.* **2005**, *44*, 8265. (d) Cano, J.; Munno, G. D.; Sanz, J. L.; Ruiz, R.; Faus, J.; Lloret, F.; Julve, M.; Caneschi, A. *J. Chem. Soc., Dalton Trans.* **1997**, 1915. (e) Hong, C. S.; You, Y. S. *Polyhedron* **2004**, *23*, 1379.

(7) (a) Maji, T. K.; Ohba, M.; Kitagawa, S. *Inorg. Chem.* **2005**, *44*, 9225. (b) Lu, J. Y.; Schauss, V. *CrystEngComm* **2002**, *4*, 623. (c) Lu, J. Y.; Schauss, V. *Inorg. Chem. Commun.* **2002**, *5*, 1028. (d) Maji, T. K.; Kaneko, W.; Ohba, M.; Kitagawa, S. *Chem. Commun.* **2005**, 4613. (e) Zheng, X. J.; Li, L. C.; Gao, S.; Jin, L. P. *Polyhedron* **2004**, *23*, 1257. (f) Chun, H.; Dybtsev, D. N.; Kim, H.; Kim, K. *Chem.−Eur. J.* **2005**, *11*, 3521. (g) Shan, N.; Bond, A. D.; Jones, W. *Tetrahedron Lett.* **2002**, *43*, 3101. (h) Bickley, J. F.; Bonar-Law, R. P.; Femoni, C.; MacLean, E. J.; Steiner, A.; Teat, S. J. *J. Chem. Soc., Dalton Trans.* **2000**, 4025. (i) Bonar-Law, R. P.; McGrath, T. D.; Singh, N.; Bickley, J. F.; Steiner, A. *Chem. Commun.* **1999**, 2457. (j) Yang, J.; Yue, Q.; Li, G.-D.; Cao, J.-J.; Li, G.-H.; Chen, J.-S. *Inorg. Chem.* **2006**, *45*, 2857.

(8) (a) Koizumi, H.; Osaki, K.; Watanabe, T. *J. Phys. Soc. Jpn.* **1963**, *18*, 117. (b) Bkouche-Waksman, I.; Bois, C.; Popovitch, G. A.; L'Haridon, P. *Bull. Soc. Chim. Fr.* **1980**, *69*, 1. (c) Kawata, T.; Uekusa, H.; Ohba, S.; Furukawa, T.; Tokii, T.; Muto, Y.; Kato, M. *Acta Crystallogr., Sect. B: Struct. Sci.* **1992**, *48*, 253. (d) Yang, R.-N.; Wang, D.-M.; Jin, D.-M.; Wang, H.-Q.; Yang, Y. *Chin. J. Struct. Chem. (Jiegou Huaxue)* **1994**, *13*, 45. (e) Yang, R.- N.; Yang, Y.-F.; Lin, K.-H.; Wang, D.-M.; Jin, D.-M.; Chen, J.; Li, M.-X. *Huaxue Xuebao (Acta Chim. Sin. (Chin. Ed.))* **1997**, *55*, 1198. (f) Murphy, B.; Aljabri, M.; Light, M.; Hursthouse, M. B. *Transition Met. Chem.* **2004**, *29*, 394. (g) Turpeinen, U.; Hamalainen, R.; Mutikainen, I. *Acta Crystallogr., Sect. C: Cryst. Struct. Commun.* **1995**, *51*, 2544. (h) Spohn, M.; Strahle, J. *Z. Kristallogr.* **1987**, *179*, 205. (i) Spohn, M.; Strahle, J. *Z. Naturforsch., Teil B* **1988**, *43*, 540. (j) Gavrilenko, K. S.; Punin, S. V.; Cador, O.; Golhen, S.; Ouahab, L.; Pavlishchuk, V. V. *J. Am. Chem. Soc.* **2005**, *127*, 12246. (k) Biradha, K.; Seward, C.; Zaworotko, M. J. *Angew. Chem., Int. Ed.* **1999**, *38*, 492.

not only affect the coordination abilities and modes of related carboxylic groups but also provide convenient conditions, from the viewpoint of geometry requirements, for the formation of the intra- and/or internetwork $\pi\cdots\pi$ stacking and C−H$\cdots\pi$ interactions. Those characteristics, therefore, may make H**L**^{1} show coordination modes different from those of the related benzene- and naphthalene-based carboxylic acids and form interesting supramolecular structures with tailored properties. On the other hand, the magneto-structural correlations have been attracting great interest, not only in the theory of magnetism but also in exploiting magnetic materials.[10] In this research area, the skillful selection of organic ligands is still very pivotal for obtaining a multinuclear magnetic coupling system. Besides, the introduction of 2,2′-bipyridyl-like bidentate chelating[1k] or 4,4′-bipyridyl-like linear bridging[1e] molecules into the reaction systems involving various carboxylic acid ligands, as auxiliary ligands, usually may generate some interesting coordination architectures.

Considering all the aspects stated above, our idea in this work is to elaborately select three kinds of ligands to construct Cu^{II}, Co^{II}, and Ni^{II} carboxylate complexes exhibiting interesting magnetic properties (see Chart 1): (1) H**L**^{1}, an analogue of H**BA**, as the primary ligand by taking the advantage of its carboxylate chelating/bridging coordination abilities together with the steric bulk of its anthracene ring; (2) two 2,2′-bipyridyl-like chelating ligands [2,2′-bipyridine (**L**^{2}) and 1,10-phenanthroline (**L**^{4})] as terminal groups; (3) two 1,4-diamine bridging ligands [1,4-diazabicyclo[2.2.2]-octane (**L**^{3}) and 4,4′-bipyridine (**L**^{5})] as a spacer in the construction of metal carboxylate polymers. Herein, we report the syntheses, crystal structures, and magnetic properties of six Cu^{II}, Co^{II}, and Ni^{II} complexes with these ligands.

Experimental Section

Materials and General Methods. All the reagents and solvents for synthesis were commercially available and were used as received or purified by standard methods prior to use. Elemental analyses (C, H, N) were performed on a Perkin-Elmer 240C analyzer. The IR spectra were recorded in the range 4000∼400 cm^{-1} on a Tensor 27 OPUS (Bruker) FT-IR spectrometer with KBr pellets.

Magnetic Studies. The variable-temperature magnetic susceptibilities were measured at the Servei de Magnetoquímica (Universitat de Barcelona) on crushed polycrystalline samples (ca. 30 mg) using a Quantum Design SQUID MPMS-XL magnetometer equipped with a 5 T magnet. The diamagnetic corrections were evaluated from Pascal's constants for all the constituent atoms. Magnetization measurements were carried out at low temperature (2 K) in the 0−5 T range.

Synthesis of the Complexes. Single crystals of **1**−**6** suitable for X-ray analysis were obtained by a method similar to that described below for **1**.

[Cu_2(L^{1})$_4$(CH_3OH)$_2$](CH_3OH) (1). A solution of H**L**^{1} (0.05 mmol) in CH_3OH (10 mL) in the presence of excess 2,6-dimethylpyridine (ca. 0.05 mL for adjusting the pH value to basic conditions) was carefully layered on top of a H_2O solution (15 mL) of $Cu(NO_3)_2\cdot 4H_2O$ (0.1 mmol) in a test tube. Black-green single crystals suitable for X-ray analysis appeared at the boundary between CH_3OH and H_2O after ca. 1 month at room temperature. Yield: ∼40% based on H**L**^{1}. Anal. Calcd for $C_{63}H_{48}Cu_2O_{11}$: C, 68.28; H, 4.37. Found: C, 68.59; H, 4.21. IR (KBr pellet, cm^{-1}): 3389(m, br), 3046(w), 2361(w), 1624(m), 1588(vs), 1522(w), 1486-(m), 1445(m), 1422(s), 1393(s), 1318(s), 1276(m), 1142(w), 1018-(w), 954(w), 890(m), 845(m), 801(w), 771(m), 727(s), 639(w), 599(m), 527(w), 491(w).

[Cu_4(L^{1})$_6$(L^{2})$_4$](NO_3)$_2$(H_2O)$_2$ (2). The same procedure as that for **1** was used for this complex except for the introduction of auxiliary ligand **L**^{2} (0.05 mmol). Yield: ∼50% based on H**L**^{1}. Anal. Calcd for $C_{130}H_{90}Cu_4N_{10}O_{20}$: C, 65.98; H, 3.83; N, 5.92. Found: C, 66.29; H, 3.54; N, 6.15. IR (KBr pellet, cm^{-1}): 3044(w), 2361-(w), 1600(w), 1577(w), 1561(vs), 1472(w), 1446(s), 1415(m), 1361-(s), 1345(s), 1300(m), 1266(m), 1170(w), 1058(w), 935(w), 864(w), 813(w), 760(s), 737(s), 726(m), 650(w), 596(w), 522(m), 412(w).

{**[Cu_2(L^{1})$_4$(L^{3})](CH_3OH)$_{0.25}$**}$_\infty$ **(3)**. The same procedure as that for **1** was used for this complex except for the introduction of auxiliary ligand **L**^{3}. Yield: ∼40% based on H**L**^{1}. Anal. Calcd for $C_{66.25}H_{49}Cu_2N_2O_{8.25}$: C, 70.28; H, 4.36; N, 2.47. Found: C, 70.55; H, 4.13; N, 2.61. IR (KBr pellet, cm^{-1}): 3444(w), 3320(m, br), 3047(w), 2361(w), 1624(w), 1588(vs), 1515(w), 1488(w), 1434-(s), 1396(m), 1320(s), 1279(m), 1060(w), 1005(w), 950(w), 868-(w), 839(m), 799(m), 770(m), 731(s), 655(w), 599(w), 527(w), 478(m).

[Co_2(L^{1})$_4$(L^{4})$_2$(μ-H_2O)](CH_3OH) (4). The same procedure as that for **1** was used for this complex except for the introduction of auxiliary ligand **L**^{4} and the use of $Co(NO_3)_2\cdot 6H_2O$ instead of $Cu(NO_3)_2\cdot 4H_2O$. Yield: ∼50% based on H**L**^{1}. Anal. Calcd for $C_{85}H_{58}Co_2N_4O_{10}$: C, 72.24; H, 4.14; N, 3.96. Found: C, 71.89; H, 4.29; N, 3.85. IR (KBr pellet, cm^{-1}): 3052(w), 2360(w), 1609(vs), 1540-(w), 1516(m), 1428(s), 1396(s), 1324(s), 1277(w), 1222(w), 1102-(w), 1035(w), 1011(w), 882(m), 861(m), 844(s), 793(w), 751(m), 728(s), 666(m), 638(w), 600(w), 558(w), 465(w), 425(w).

{**[Co(L^{1})$_2$(L^{5})(CH_3OH)$_2$]**}$_\infty$ **(5)**. The same procedure as that for **1** was used for this complex except for the introduction of auxiliary ligand **L**^{5} and the use of $Co(NO_3)_2\cdot 6H_2O$ instead of $Cu(NO_3)_2\cdot 4H_2O$. Yield: ∼40% based on H**L**^{1}. Anal. Calcd for $C_{42}H_{34}CoN_2O_6$: C, 69.90; H, 4.75; N, 3.88. Found: C, 70.07; H, 4.93; N, 3.71. IR (KBr pellet, cm^{-1}): 3056(w), 2360(w), 1572(vs), 1484-(w), 1441(m), 1389(s), 1319(s), 1273(m), 1217(m), 1137(w), 1069-(m), 1037(w), 1004(w), 885(m), 862(s), 841(m), 733(vs), 664(s), 627(m), 560(w), 524(w), 458(w), 419(w).

{**[Ni(L^{1})$_2$(L^{5})(CH_3OH)$_2$]**}$_\infty$ **(6)**. The same procedure as that for **1** was used for this complex except for the introduction of auxiliary ligand **L**^{5} and the use of $Ni(NO_3)_2\cdot 6H_2O$ instead of $Cu(NO_3)_2\cdot 4H_2O$. Yield: ∼40% based on H**L**^{1}. Anal. Calcd for $C_{42}H_{34}NiN_2O_6$: C, 69.93; H, 4.75; N, 3.88. Found: C, 69.79; H, 4.89; N, 3.69. IR (KBr pellet, cm^{-1}): 3412(w), 3057(w), 1570(vs), 1483(w), 1441-(m), 1396(s), 1319(s), 1273(m), 1217(m), 1140(m), 1070(w), 1038-(m), 1006(w), 884(m), 863(s), 841(m), 793(s), 760(m), 732(vs), 664(m), 629(m), 600(w), 577(w), 527(w), 461(w), 421(w).

(9) (a) Liu, C.-S.; Shi, X.-S.; Li, J.-R.; Wang, J.-J.; Bu, X.-H. *Cryst. Growth Des.* **2006**, *6*, 656. (b) Zou, R.-Q.; Liu, C.-S.; Shi, X.-S.; Bu, X.-H.; Ribas, J. *CrystEngComm* **2005**, *7*, 722. (c) Bu, X.-H.; Tong, M.-L.; Chang, H.-C.; Kitagawa, S.; Batten, S. R. *Angew. Chem., Int. Ed.* **2004**, *43*, 192. (d) Bu, X.-H.; Tong, M.-L.; Xie, Y.-B.; Li, J.-R.; Chang, H.-C.; Kitagawa, S.; Ribas, J. *Inorg. Chem.* **2005**, *44*, 9837.

(10) For examples see: (a) Monfort, M.; Resino, I.; Ribas, J.; Solans, X.; Font-Bardia, M.; Rabu, P.; Drillon, M. *Inorg. Chem.* **2000**, *39*, 2572. (b) Gutschke, S. O. H.; Price, D. J.; Powell, A. K.; Wood, P. T. *Angew. Chem., Int. Ed.* **2001**, *113*, 1974. (c) Du, M.; Guo, Y. M.; Bu, X. H.; Ribas, J.; Monfort, M. *New J. Chem.* **2002**, *5*, 645. (d) Yoon, J.; Mirica, L. M.; Stack, T. D. P.; Solomon, E. I. *J. Am. Chem. Soc.* **2004**, *126*, 12586. (e) Zhao, M.; Zhong, C.; Stern, C.; Barrett, A. G. M.; Hoffman, B. M. *J. Am. Chem. Soc.* **2005**, *127*, 9769. (f) Triki, S.; Gomez-Garcia, C. J.; Ruiz, E.; Sala-Pala, J. *Inorg. Chem.* **2005**, *44*, 5501.

X-ray Data Collection and Structure Determinations. X-ray single-crystal diffraction data for complexes **1**−**6** were collected on a Bruker Smart 1000 CCD area-detector diffractometer at 293(2) K with Mo Kα radiation ($\lambda = 0.71073$ Å) in the ω scan mode. The program SAINT[11] was used for integration of the diffraction profiles. Semiempirical absorption corrections were applied using the SADABS program.[12] All the structures were solved by direct methods using the SHELXS program of the SHELXTL package and refined by full-matrix least-squares methods with SHELXL.[13] Metal atoms in each complex were located from the *E* maps, and the other non-hydrogen atoms were located in successive difference Fourier syntheses and refined with anisotropic thermal parameters on F^2. The hydrogen atoms except for those of H_2O and partial CH_3OH molecules in each complex were generated theoretically on the specific atoms and refined with isotropic thermal parameters riding on the parent atoms. The hydrogen atoms of the H_2O and partial CH_3OH molecules in **1**, **4**, **5**, and **6** were added by difference Fourier *E* maps and refined isotropically. For **3**, the conformationally disordered **L**^{4} ligand was treated with split-atom models. Also, disordered NO_3^- groups were found in complex **2**, and a suitable site occupation separation was used for the refinement in such a case. Further details for structural analysis are summarized in Table 1.

X-ray Powder Diffraction. The X-ray powder diffraction (XRPD) patterns of **1**−**6** were recorded on a Rigaku D/Max-2500 diffractometer, operated at 40 kV and 100 mA, using a Cu target tube and a graphite monochromator. The intensity data were recorded by continuous scan in the $2\theta/\theta$ mode from 3° to 80° with a step size of 0.02° and a scan speed of 8° min^{-1}. Simulation of the XRPD spectra was carried out by the single-crystal data and diffraction-crystal module of the Mercury (Hg) program available free of charge via the Internet at http://www.iucr.org.

Results and Discussion

Synthesis Consideration and General Characterization. For a systematic investigation of the Cu^{II}, Co^{II}, and Ni^{II} complexes with H**L**^{1}, our strategy was to obtain qualified crystals suitable for X-ray diffraction analysis by changing the auxiliary ligands including bidentate chelating ligands (**L**^{2} and **L**^{4}) or linear bridging ligands (**L**^{3} and **L**^{5}). It should be pointed out that the self-assembly processes are usually influenced by many factors, such as the metal:ligand ratio, counteranion, reaction pH, and versatility of the metal coordination geometry. Therefore, properly lowering the reaction speed may often result in the formation of crystalline products to facilitate the slow growth of well-shaped larger single crystals suitable for X-ray diffraction.[14] Considering this point, the synthesis and isolation of **1**−**6** in this work were carried out through self-assembly reaction of Cu^{II}, Co^{II}, or Ni^{II} salts with H**L**^{1}, together with the introduction of different auxiliary ligands, **L**^{2}, **L**^{3}, **L**^{4}, or **L**^{5} (except **1**), by using the slow diffusion method in a test tube under mild conditions of ambient temperature and pressure. Also, single crystals obtained from the slow diffusion method may often be the kinetic products. Besides, the use of excess 2,6-dimethylpyridine is a key point for the formation of **1**−**6**, which adjusts the pH values of the reaction systems.

Table 1. Crystallographic Data and Structure Refinement Summary for Complexes **1**−**6**

	1	**2**	**3**
empirical formula	$C_{63}H_{48}Cu_2O_{11}$	$C_{130}H_{90}Cu_4N_{10}O_{20}$	$C_{66.25}H_{49}Cu_2N_2O_{8.25}$
fw	1108.09	2366.28	1132.15
cryst syst	orthorhombic	monoclinic	tetragonal
space group	*Pccn*	*C*2/*c*	*P*4/*nnc*
a/Å	24.654(15)	22.086(2)	16.856(2)
b/Å	50.52(3)	19.7292(17)	16.856(2)
c/Å	8.581(5)	24.662(2)	9.4198(19)
α/deg	90	90	90
β/deg	90	95.933(6)	90
γ/deg	90	90	90
V/Å^3	10688(11)	10688.4(16)	2676.4(8)
Z	8	4	2
D/g cm^{-3}	1.377	1.470	1.405
μ/mm^{-1}	0.859	0.865	0.856
GOF	0.880	0.985	1.222
T/K	293(2)	293(2)	293(2)
R1[a]/wR2[b]	0.0549/0.1054	0.0563/0.1626	0.0454/0.1070

	4	**5**	**6**
empirical formula	$C_{85}H_{58}Co_2N_4O_{10}$	$C_{42}H_{34}CoN_2O_6$	$C_{42}H_{34}NiN_2O_6$
fw	1413.21	721.64	721.42
cryst syst	triclinic	monoclinic	monoclinic
space group	$P\bar{1}$	*C*2/*c*	*C*2/*c*
a/Å	14.628(3)	23.999(5)	24.075(5)
b/Å	15.021(3)	11.498(2)	11.397(2)
c/Å	17.985(4)	11.968(2)	12.050(2)
α/deg	70.51(3)	90	90
β/deg	71.64(3)	95.26(3)	94.356(3)
γ/deg	65.42(3)	90	90
V/Å^3	3315.5(15)	3288.3(11)	3296.7(12)
Z	2	4	4
D/g cm^{-3}	1.416	1.458	1.454
μ/mm^{-1}	0.569	0.578	0.644
GOF	1.087	1.067	1.061
T/K	293(2)	293(2)	293(2)
R1[a]/wR2[b]	0.0669/0.1853	0.0272/0.0750	0.0543/0.1394

[a] $R1 = \sum(||F_o| - |F_c||)/\sum|F_o|$. [b] $wR2 = [\sum w(|F_o|^2 - |F_c|^2)^2/\sum w(F_o^2)]^{1/2}$.

Complexes **1**−**6** are all air stable. In general, the IR spectra show features attributable to each component of the complexes,[15] and the characteristic bands of the carboxylate groups appeared in the usual region at 1609−1561 cm^{-1} for the antisymmetric stretching vibrations and at 1446−1361 cm^{-1} for the symmetric stretching vibrations. Furthermore, the $\Delta\nu$ values [$\Delta\nu = \nu_{as}(COO^-) - \nu_s(COO^-)$] are 166 cm^{-1} for **1**, 115, 200, and 216 cm^{-1} for **2**, 154 cm^{-1} for **3**, 181 and 213 cm^{-1} for **4**, 183 cm^{-1} for **5**, and 174 cm^{-1} for **6**, in good agreement with their solid structural features from the results of crystal structures.[16] Therefore, the corresponding IR results are well coincident with the crystallographic structural analyses. As such, the elemental analyses are also consistent with the results of the structural analysis.

(11) *SAINT Software Reference Manual*; Bruker AXS: Madison, WI, 1998.
(12) Sheldrick, G. M. *SADABS, Siemens Area Detector Absorption Corrected Software*; University of Göttingen: Göttingen, Germany, 1996.
(13) Sheldrick, G. M. *SHELXTL NT Version 5.1. Program for Solution and Refinement of Crystal Structures*; University of Göttingen: Göttingen, Germany, 1997.
(14) Wilkinson, G., Gillard, R. D., McCleverty, J. A., Eds. *Comprehensive Coordination Chemistry*; Pergamon: Oxford, U.K., 1987; Vol. 5.
(15) Nakamoto, K. *Infrared and Raman Spectra of Inorganic and donor hydrogen bond Coordination Compounds*; John Wiley & Sons: New York, 1986.
(16) (a) Deacon, G. B.; Phillips, R. J. *Coord. Chem. Rev.* **1980**, *33*, 227. (b) Du, M.; Zhang, Z.-H.; Zhao, X.-J.; Xu, Q. *Inorg. Chem.* **2006**, *45*, 5785.

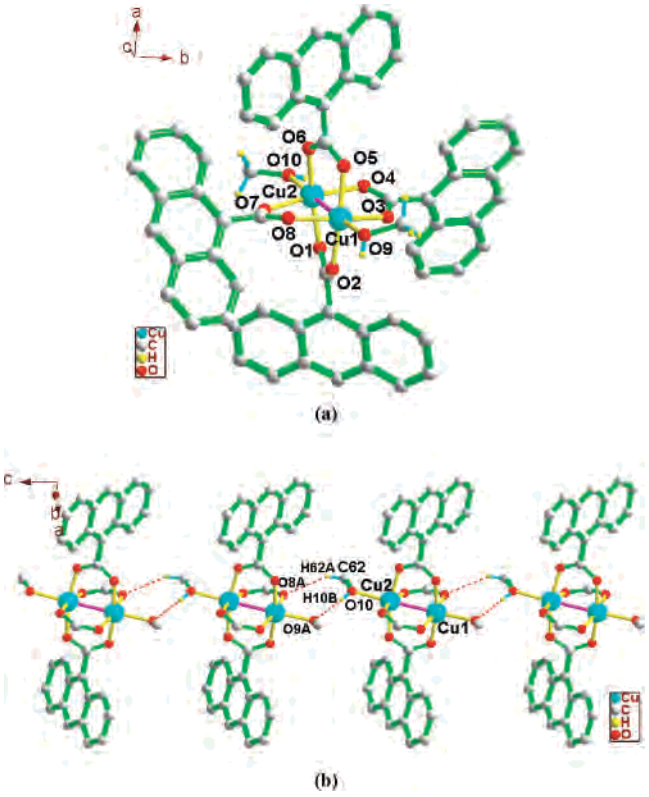

Figure 1. View of (a) the coordination environment of Cu^{II} in the dinuclear unit of **1** and (b) the 1D chain in **1** formed by intermolecular C−H···O H-bonding interactions between the dinuclear units (orange dashed lines) (partial H atoms and anthracene rings of the **L^1** ligands were omitted for clarity).

Descriptions of Crystal Structures for 1−6. [Cu$_2$(L^1)$_4$(CH$_3$OH)$_2$](CH$_3$OH) (1). The structure of **1** consists of a paddle-wheel-shaped dinuclear unit, [Cu$_2$(**L^1**)$_4$(CH$_3$OH)$_2$], and the free CH$_3$OH molecule (Figure 1a). In the dinuclear unit, there are two crystallographically distinct Cu^{II} centers [Cu(1) and Cu(2)] mainly in the aspects of bond distances and angles bridged by four carboxylate groups of four distinct **L^1** ligands (**L^1** = anthracene-9-carboxylate); however, they have the same coordination environment. If the Cu−Cu bonding contact is neglected, each Cu^{II} center is pentacoordinated to four O atoms of carboxylate groups from four distinct **L^1** ligands (the average Cu−O distance being 1.971 Å) in the equatorial plane and one O atom of the CH$_3$OH molecule locating at the axial position. The τ[17] values are 0.044 and 0.047 (thus, close to 0) for Cu(1) and Cu(2) in **1**, indicating an almost ideal square-pyramid coordination environment, and the Cu(1) and Cu(2) ions deviate from the mean equatorial plane of the square pyramid toward the apical O(9) and O(10) atoms by ca. 0.1820 and 0.2092 Å, respectively. Interestingly, the Cu−Cu distance of 2.608(2) Å in the dinuclear unit is well below the summed van der Waals radii of two Cu atoms (2.8 Å) but is slightly longer than the Cu−Cu separation of 2.56 Å in metallic copper.[18] Also, all the Cu−O bond distances and the angles around each Cu^{II} center are in the normal range expected for such coordination complexes (see Table 2).[19] Moreover, **L^1** in **1** adopts a bidentate *syn*−*syn* bridging coordination mode (Scheme 1a) using two O atoms of the carboxylate group, and the dihedral angles between the carboxylate planes and the anthracene groups range from 59.8° to 117.9°.

Table 2. Selected Bond Distances (Å) and Angles (deg) for Complex **1**

Cu(1)−O(5)	1.955(3)	Cu(1)−O(8)	1.963(3)
Cu(1)−O(3)	1.973(3)	Cu(1)−O(2)	1.985(3)
Cu(1)−O(9)	2.188(3)	Cu(1)−Cu(2)	2.6079(17)
Cu(2)−O(6)	1.959(3)	Cu(2)−O(4)	1.964(3)
Cu(2)−O(7)	1.970(3)	Cu(2)−O(1)	2.001(3)
Cu(2)−O(10)	2.154(4)		
O(5)−Cu(1)−O(8)	89.71(13)	O(5)−Cu(1)−O(3)	91.01(13)
O(8)−Cu(1)−O(3)	168.01(13)	O(5)−Cu(1)−O(2)	170.65(13)
O(8)−Cu(1)−O(2)	88.94(13)	O(3)−Cu(1)−O(2)	88.41(13)
O(5)−Cu(1)−O(9)	92.45(12)	O(8)−Cu(1)−O(9)	97.28(13)
O(3)−Cu(1)−O(9)	94.65(13)	O(2)−Cu(1)−O(9)	96.90(13)
O(5)−Cu(1)−Cu(2)	84.78(9)	O(8)−Cu(1)−Cu(2)	83.87(9)
O(3)−Cu(1)−Cu(2)	84.28(10)	O(2)−Cu(1)−Cu(2)	85.87(9)
O(9)−Cu(1)−Cu(2)	177.01(9)	O(6)−Cu(2)−O(4)	91.85(13)
O(6)−Cu(2)−O(7)	89.90(13)	O(4)−Cu(2)−O(7)	169.03(13)
O(6)−Cu(2)−O(1)	166.20(12)	O(4)−Cu(2)−O(1)	87.45(13)
O(7)−Cu(2)−O(1)	88.28(12)	O(6)−Cu(2)−O(10)	95.29(13)
O(4)−Cu(2)−O(10)	95.39(14)	O(7)−Cu(2)−O(10)	95.23(14)
O(1)−Cu(2)−O(10)	98.50(13)	O(6)−Cu(2)−Cu(1)	83.47(9)
O(4)−Cu(2)−Cu(1)	84.61(9)	O(7)−Cu(2)−Cu(1)	84.83(10)
O(1)−Cu(2)−Cu(1)	82.75(8)	O(10)−Cu(2)−Cu(1)	178.75(10)

Scheme 1. Coordination Modes of the H**L^1** Ligand in **1**−**6**: (a) *syn*−*syn* Bridging; (b) Unidentate; (c) μ-O,O′$_{anti}$−μ-O,O

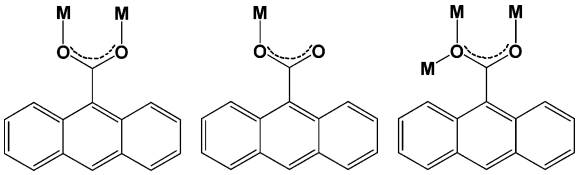

In addition, the adjacent discrete dinuclear [Cu$_2$(**L^1**)$_4$(CH$_3$OH)$_2$] molecules are arranged into a 1D chain by intermolecular C−H···O H-bonding between O(8A) and H(62A) of **L^1** and the coordinated CH$_3$OH (for more information, see Figure 1b and Table 7).[20] Furthermore, the adjacent anthracene rings from different dinuclear units are aligned in an offset fashion, being approximately parallel to each other with a center−center distance of ca. 3.586 Å, an average interplanar separation of 3.526 Å, and a dihedral angle of 6.3°, indicating the presence of face-to-face π···π stacking[21] and thus resulting in a 2D network (see Figure S1 in the Supporting Information).

[Cu$_4$(L^1)$_6$(L^2)$_4$](NO$_3$)$_2$(H$_2$O)$_2$ (2). Different from **1**, the structure of **2** is a centrosymmetric tetranuclear motif consisting of discrete [Cu$_2$(**L^1**)$_3$(**L^2**)$_2$]$_2^{2+}$ cations, NO$_3^-$, and

(17) Addison, A. W.; Rao, T. N.; Reedijk, J.; van Rijn, J.; Verschoor, G. C. *J. Chem. Soc., Dalton Trans.* **1984**, 1349.
(18) Jones, P. L.; Jeffery, J. C.; Maher, J. P.; McCleverty, J. A.; Rieger, P. H.; Ward, M. D. *Inorg. Chem.* **1997**, *36*, 3088.
(19) (a) Orpen, A. G.; Brammer, L.; Allen, F. H.; Kennard, O.; Watson, D. G.; Taylor, R. *J. Chem. Soc., Dalton Trans.* **1989**, S1. (b) Allen, F. H.; Kennard, O.; Watson, D. G.; Brammer, L.; Orpen, A. G.; Taylor, R. *J. Chem. Soc., Perkin Trans. 2* **1987**, S1. (c) O Keeffe, M.; Brese, N. E. *J. Am. Chem. Soc.* **1991**, *113*, 3226.
(20) (a) Desiraju, G. R.; Steiner, T. *The Weak Hydrogen Bond in Structural Chemistry and Biology*; Oxford University Press: Oxford, 1999. (b) Calhorda, M. J. *Chem. Commun.* **2000**, 801. (c) Hobza, P.; Havlas, Z. *Chem. Rev.* **2000**, *100*, 4253. (d) Steiner, T *Chem. Commun.* **1997**, 727. (e) Desiraju, G. R. *Chem. Commun.* **2005**, 2995 and references therein.
(21) (a) Janiak, C. *J. Chem. Soc., Dalton Trans.* **2000**, 3885. (b) Sony, S. M. M.; Ponnuswamy, M. N. *Cryst. Growth Des.* **2006**, *6*, 736 and references therein.

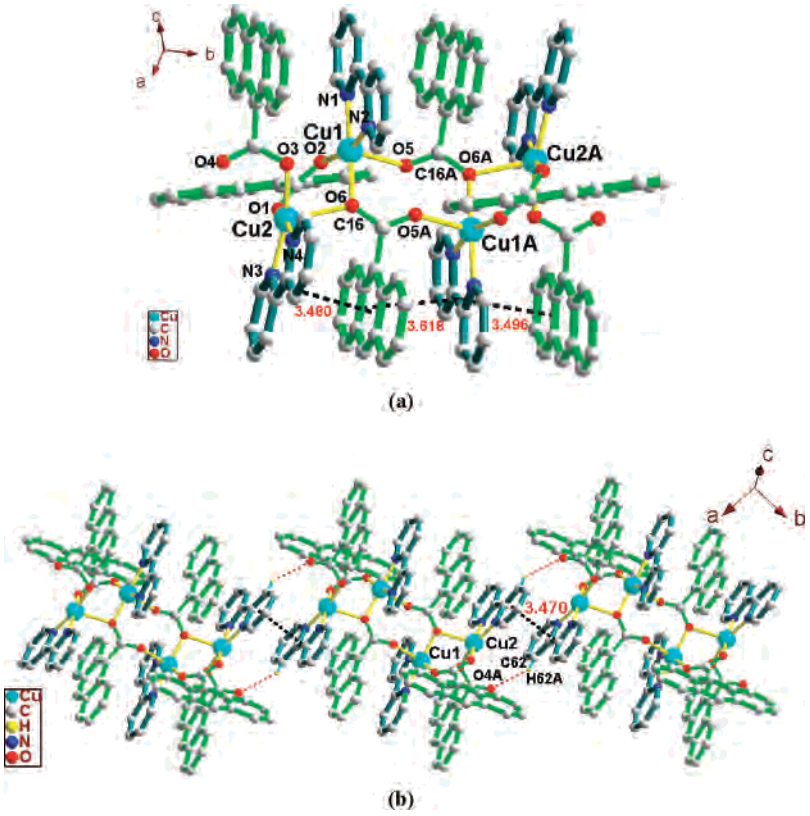

Figure 2. View of (a) the coordination environment of Cu^{II} in the tetranuclear unit of **2** showing intramolecular $\pi\cdots\pi$ stacking interactions (black dashed lines) and (b) the 1D chain in **2** formed by intermolecular $\pi\cdots\pi$ stacking (black dashed lines) and C−H···O H-bonding (orange dashed lines) interactions between the tetranuclear units (uncoordinated NO_3^- anions, free H_2O molecules, and partial H atoms were omitted for clarity).

Table 3. Selected Bond Distances (Å) and Angles (deg) for Complex **2**

Cu(1)−O(6)	1.975(3)	Cu(1)−O(2)	1.997(3)
Cu(1)−N(1)	2.004(4)	Cu(1)−N(2)	2.015(4)
Cu(1)−O(5)	2.376(3)	Cu(2)−O(1)	1.919(3)
Cu(2)−O(3)	1.972(3)	Cu(2)−N(4)	1.992(4)
Cu(2)−N(3)	2.007(4)	Cu(2)−O(6)	2.302(3)
O(6)−Cu(1)−O(2)	92.77(13)	O(6)−Cu(1)−N(1)	178.65(14)
O(2)−Cu(1)−N(1)	87.68(16)	O(6)−Cu(1)−N(2)	98.14(15)
O(2)−Cu(1)−N(2)	164.32(15)	N(1)−Cu(1)−N(2)	81.16(17)
O(6)−Cu(1)−O(5)	84.90(11)	O(2)−Cu(1)−O(5)	83.95(12)
N(1)−Cu(1)−O(5)	96.40(13)	N(2)−Cu(1)−O(5)	108.11(13)
O(1)−Cu(2)−O(3)	94.22(14)	O(1)−Cu(2)−N(4)	169.05(16)
O(3)−Cu(2)−N(4)	96.54(16)	O(1)−Cu(2)−N(3)	88.37(16)
O(3)−Cu(2)−N(3)	165.69(14)	N(4)−Cu(2)−N(3)	80.71(17)
O(1)−Cu(2)−O(6)	93.52(13)	O(3)−Cu(2)−O(6)	78.93(12)
N(4)−Cu(2)−O(6)	90.53(14)	N(3)−Cu(2)−O(6)	115.00(13)

free H_2O. There are two Cu^{II} centers [Cu(1) and Cu(2)] in the asymmetric unit (Figure 2a). Each Cu^{II} is five-coordinated by two N donors from one chelating $\mathbf{L^2}$ and three O atoms from three distinct $\mathbf{L^1}$ ligands and has slight differences in bond distances and angles (see Table 3). The τ value here is 0.056 for Cu(2), also indicating an almost ideal square-pyramid coordination environment, and the Cu(1) and Cu(2) ions deviate from the mean equatorial plane of the square pyramid toward the apical O(5) and O(6) atoms by ca. 0.1071 and 0.1280 Å, respectively. $\mathbf{L^2}$ acts as a typical chelating ligand coordinating to Cu^{II} ions. For $\mathbf{L^1}$, there exist three different kinds of carboxylic coordination modes with Cu^{II}, namely, *syn*−*syn* bridging (see Scheme 1a), unidentate (see Scheme 1b), and μ-O,O′$_{anti}$−μ-O,O (see Scheme 1c) coordination modes, which further connect the different Cu^{II} ions to form a nonplanar six-membered ring composed of Cu(1)−O(6)−Cu(2)−O(1)−C(1)−O(2) with a nonbonding Cu(1)···Cu(2) separation of 3.287(4) Å and also an eight-membered ring consisting of Cu(1)−O(6)−C(16A)−O(5A)−Cu(1A)−O(6A)−C(16)−O(5) with a nonbonding Cu(1)···Cu(1A) separation of 4.979(1) Å. It should be pointed out that the existence of intramolecular face-to-face $\pi\cdots\pi$ stacking was observed between anthracene and pyridine rings of $\mathbf{L^1}$ and $\mathbf{L^2}$ (the centroid−centroid separations, the interplanar separations, and the dihedral angles range from 3.480 to 3.618 Å, from 3.4028 to 3.5539 Å, and from 0.6° to 6.2°, respectively) (Figure 2a).[21]

Additionally, the adjacent tetranuclear $[Cu_2(\mathbf{L^1})_3(\mathbf{L^2})_2]_2^{2+}$ units are arranged into a 1D chain by the coeffects of the intermolecular $\pi\cdots\pi$ stacking and C−H···O H-bonding (see Figure 2b and Table 7)[20] between the pyridine rings from adjacent $\mathbf{L^2}$ ligands. The centroid−centroid and average interplanar separations are 3.470 and 3.4623 Å, with the dihedral angle between them being 2.0°.

In addition to the obvious intra- and intermolecular weak interactions, such as H-bonding and $\pi\cdots\pi$ stacking mentioned above, the structure also contains numerous intra- and internetwork C−H···π supramolecular interactions between the anthracene rings with an edge-to-face orientation that further link low-dimensional 1D chain entities into a 2D sheet and then a 3D supramolecular network from different crystallographic directions (d = 2.6742, 2.9172, and 3.1063 Å and A = 173.67°, 153.76°, and 174.86° in the C−H···π

patterns; *d* and *A* stand for the H···π separations and C−H···π angles in the C−H···π patterns, respectively] (see Figure S2 in the Supporting Information).[21]

On the basis of the above results, it can be seen that the introduction of **L^2** has obviously affected the formation and the final crystal packing of **2** (dinuclear structure for **1** and tetranuclear structure for **2**) because chelating 2,2′-bipyridine often has a great influence on the self-assembly process of aromatic acids with transition-metal ions, which often can reduce the available metal ion binding sites from carboxylate ligands and favor formation of a single-metal center and/or a metal cluster.[1k] Besides, the bulky anthracene ring skeleton in **2** not only surrounds all the O atoms of the carboxylate groups of **L^1** ligands within their open shell sphere but also presumably provides convenient conditions, from the viewpoint of geometry requirements, for the formation of the intermolecular C−H···π interactions between the centrosymmetric tetranuclear units.

{[Cu$_2$(L^1)$_4$(L^3)](CH$_3$OH)$_{0.25}$}$_\infty$ (3). Different from **1** and **2**, the structure of **3** consists of free CH_3OH and infinite 1D neutral chains containing centrosymmetric dinuclear [Cu_2-(L^1)$_4$(L^3)$_2$] units as nodes (Figure 3a,b). In the centrosymmetric dinuclear unit, there are two completely crystallographically equal Cu^{II} centers [Cu(1) and Cu(1A)] bridged by four carboxylate groups of four distinct **L^1** ligands. If the Cu−Cu bonding contact is neglected, each Cu^{II} is pentacoordinated to four oxygen atoms of carboxylate groups from different ligands [Cu−O 1.9730(2) Å] in the equatorial plane and one N donor of the **L^3** ligand locating at the axial position [Cu−N 2.164(5) Å] (see Table 4). In the equatorial position of **3**, all the Cu−O bond distances are the same probably due to having a crystallographic 4-fold rotation axis (space group *P4/nnc*). The τ value is 0 for Cu(1),[17] indicating a completely ideal square-pyramid coordination environment, and the Cu(1) ion deviates from the mean equatorial plane of the square pyramid toward the apical N(1) donor by ca. 0.2015 Å. Similar to **1**, the Cu−Cu distance of 2.5639(1) Å in the dinuclear unit of **3** is also below the summed van der Waals radii of two Cu atoms (2.8 Å) but is slightly longer than the Cu−Cu separation of 2.56 Å in metallic copper.[18] Moreover, in **3**, **L^1** adopts a *syn*−*syn* bridging mode using two O atoms of the carboxylate group (see Scheme 1a) and the dihedral angle between the carboxylate planes and the anthracene groups is 53.5°.

Besides, the adjacent 1D chains are further linked together to form a 2D sheet and then a 3D network from the diagonal direction of the *a* and *b* axes, respectively, by interchain π···π stacking between completely parallel anthracene rings in an offset fashion with a centroid−centroid separation of 3.666 Å and an interplanar separation of 3.3996 Å (see Figure 3c and Figure S3 in the Supporting Information). In fact, if viewed along the *c* axis, the structure of **3** in the *ab* plane could be regarded as a (4,4) 2D sheet formed by interchain π···π stacking interactions, which are further linked into a 3D network via head-to-end bridging **L^3** ligands (Figure 3c).

[Co$_2$(L^1)$_4$(L^4)$_2$(μ-H$_2$O)](CH$_3$OH) (4). The structure of **4** consists of a centrosymmetric dinuclear unit **[**Co_2(**L^1**)$_4$(**L^4**)$_2$-(μ-H_2O)**]** with a central Co^{II} ion six-coordinated by two N

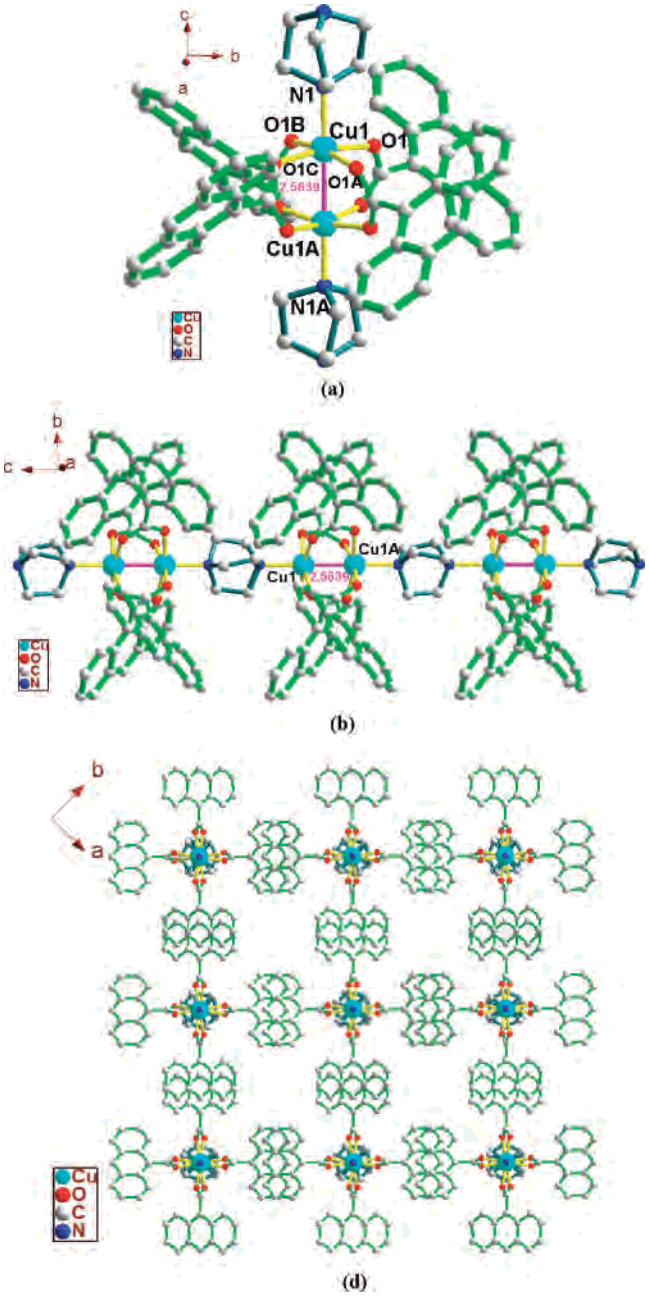

Figure 3. View of (a) the coordination environment of Cu^{II} in the dinuclear unit of **3**, (b) the 1D chain, and (c) the 3D supramolecular network showing a 4,4 (2D) planar sheet viewed along the *c* direction formed by interchain π···π stacking interactions from the diagonal directions of the *a* and *b* axes (free CH_3OH molecules and H atoms were omitted for clarity).

donors from one chelating **L^4** ligand, three O atoms from three **L^1** ligands, and one O atom from a μ-H_2O molecule (Figure 4a). **L^4** acts as a typical chelating ligand coordinating to Co^{II} with Co−N bond distances ranging from 2.112(3) to 2.177(3) Å and N−Co−N angles of 78.11(1)° and 77.85-(1)° (see Table 5). For **L^1**, there exist two different kinds of carboxylic coordination modes with Co^{II}, namely, *syn*−*syn* bridging (μ_2-η^1:η^1-bridging) and unidentate modes (see Scheme 1a,b) to connect two Co^{II} ions to form an eight-membered ring composed of Co(1)−O(7)−C(1)−O(8)−Co-(2)−O(5)−C(16)−O(6) with a nonbonding Co···Co separation of 3.566 Å. As such, each μ-H_2O also interlinks two crystallographically unique Co^{II} ions [Co(1)−O(1W) 2.162-

Table 4. Selected Bond Distances (Å) and Angles (deg) for Complex **3**[a]

Cu(1)−O(1)$^{\#1}$	1.9730(19)	Cu(1)−O(1)	1.9730(19)
Cu(1)−O(1)$^{\#2}$	1.9730(19)	Cu(1)−O(1)$^{\#3}$	1.9730(19)
Cu(1)−N(1)	2.164(5)	Cu(1)−Cu(1)$^{\#4}$	2.5639(14)
O(1)$^{\#1}$−Cu(1)−O(1)	168.28(12)	O(1)$^{\#1}$−Cu(1)−O(1)$^{\#2}$	89.402(13)
O(1)−Cu(1)−O(1)$^{\#2}$	89.402(13)	O(1)$^{\#1}$−Cu(1)−O(1)$^{\#3}$	89.402(13)
O(1)−Cu(1)−O(1)$^{\#3}$	89.402(13)	O(1)$^{\#2}$−Cu(1)−O(1)$^{\#3}$	68.28(12)
O(1)$^{\#1}$−Cu(1)−N(1)	95.86(6)	O(1)−Cu(1)−N(1)	95.86(6)
O(1)$^{\#2}$−Cu(1)−N(1)	95.86(6)	O(1)$^{\#3}$−Cu(1)−N(1)	95.86(6)
O(1)$^{\#1}$−Cu(1)−Cu(1)$^{\#4}$	84.14(6)	O(1)−Cu(1)−Cu(1)$^{\#4}$	84.14(6)
O(1)$^{\#2}$−Cu(1)−Cu(1)$^{\#4}$	84.14(6)	O(1)$^{\#3}$−Cu(1)−Cu(1)$^{\#4}$	84.14(6)
N(1)−Cu(1)−Cu(1)$^{\#4}$	180.0		

[a] Symmetry codes for **3**: #1, $-x + 1/2$, $-y + 1/2$, z; #2, $-x + 1/2$, y, z; #3, x, $-y + 1/2$, z; #4, $-x + 1/2$, y, $-z + 3/2$.

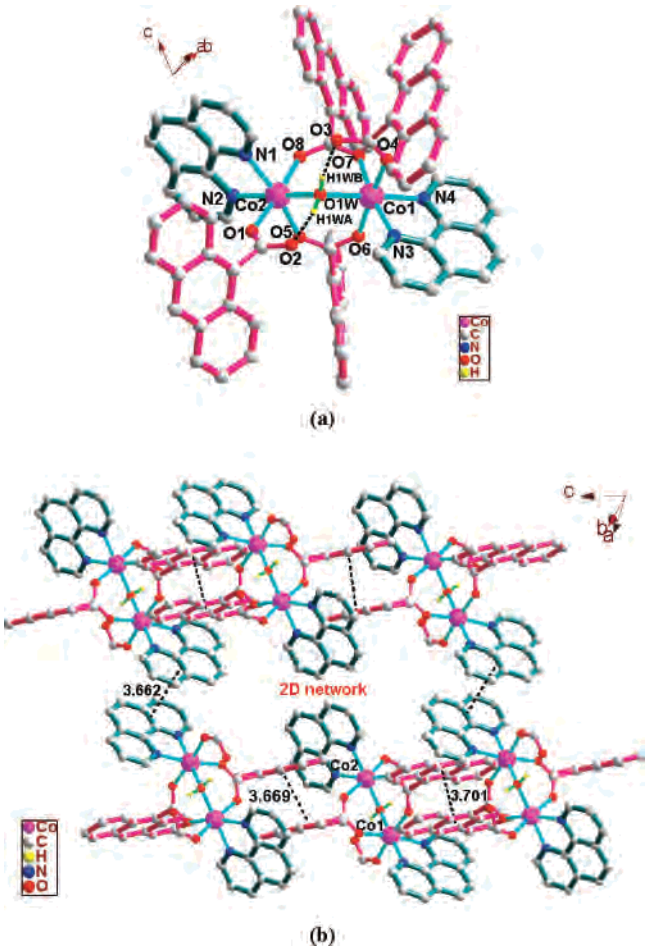

Figure 4. View of (a) the coordination environment of Co^{II} in the dinuclear unit of **4** showing the intramolecular O−H···O H-bonding (black dashed lines) and (b) the 2D network formed by intermolecular $\pi\cdots\pi$ stacking interactions between the anthracene and phenanthroline rings from different crystallographic directions (black dashed lines) (partial H atoms and anthracene rings of the $\mathbf{L^1}$ ligands were omitted for clarity).

(2) Å, Co(2)−O(1W) 2.133(2) Å], which further stabilizes the adopted dinuclear structure. It is worth noting that O(1W) of the μ-H_2O molecule presents a strong intramolecular H-bonding with O(2) and O(3) of two distinct $\mathbf{L^1}$ ligands (see Figure 4a and Table 7).[20]

In addition, the adjacent dinuclear $[Co_2(\mathbf{L^1})_4(\mathbf{L^4})_2(\mu\text{-}H_2O)]$ units are arranged into two different 1D chains from different crystallographic directions by intermolecular $\pi\cdots\pi$ stacking between the almost completely parallel anthracene rings (see

Table 5. Selected Bond Distances (Å) and Angles (deg) for Complex **4**

Co(1)−O(6)	2.040(2)	Co(1)−O(4)	2.067(2)
Co(1)−O(7)	2.073(2)	Co(1)−N(4)	2.116(3)
Co(1)−O(1W)	2.162(2)	Co(1)−N(3)	2.174(3)
Co(2)−O(8)	2.058(2)	Co(2)−O(5)	2.064(2)
Co(2)−O(1)	2.103(2)	Co(2)−N(2)	2.112(3)
Co(2)−O(1W)	2.133(2)	Co(2)−N(1)	2.177(3)
O(6)−Co(1)−O(4)	174.03(10)	O(6)−Co(1)−O(7)	95.90(11)
O(4)−Co(1)−O(7)	89.88(10)	O(6)−Co(1)−N(4)	88.56(10)
O(4)−Co(1)−N(4)	89.75(10)	O(7)−Co(1)−N(4)	91.99(10)
O(6)−Co(1)−O(1W)	94.69(10)	O(4)−Co(1)−O(1W)	86.47(10)
O(7)−Co(1)−O(1W)	93.06(9)	N(4)−Co(1)−O(1W)	173.69(10)
O(6)−Co(1)−N(3)	86.52(11)	O(4)−Co(1)−N(3)	87.54(11)
O(7)−Co(1)−N(3)	169.52(10)	N(4)−Co(1)−N(3)	77.85(11)
O(1W)−Co(1)−N(3)	96.91(10)	O(8)−Co(2)−O(5)	96.10(10)
O(8)−Co(2)−O(1)	173.51(10)	O(5)−Co(2)−O(1)	90.32(10)
O(8)−Co(2)−N(2)	90.09(10)	O(5)−Co(2)−N(2)	91.00(10)
O(1)−Co(2)−N(2)	88.83(10)	O(8)−Co(2)−O(1W)	93.00(9)
O(5)−Co(2)−O(1W)	93.25(10)	O(1)−Co(2)−O(1W)	87.58(9)
N(2)−Co(2)−O(1W)	174.45(10)	O(8)−Co(2)−N(1)	86.61(11)
O(5)−Co(2)−N(1)	168.81(10)	O(1)−Co(2)−N(1)	86.90(11)
N(2)−Co(2)−N(1)	78.11(11)	O(1W)−Co(2)−N(1)	97.45(10)

Figure S4a in the Supporting Information) or phenanthroline rings (see Figure S4b in the Supporting Information) from distinct $\mathbf{L^1}$ or $\mathbf{L^4}$ ligands, respectively, resulting in a 2D network (see Figure 4b). The centroid−centroid and average interplanar separations range from 3.660 to 3.701 Å and from 3.3831 to 3.4995 Å.[21] Moreover, **4** also contains numerous intra- and/or internetwork C−H···π supramolecular interactions between the anthracene and phenanthroline rings with an edge-to-face orientation that further link the low-dimensional 1D chain entities into a higher-dimensional supramolecular network from different crystallographic directions (d = 2.8318, 2.9049, 2.9537, 2.9702, and 2.9920 Å and A = 137.47°, 133.55°, 133.83°, 139.54°, and 146.99° in the C−H···π patterns) (see Figure S4c in the Supporting Information).[21]

Two 1D Chain Complexes, $\{[Co(\mathbf{L^1})_2(\mathbf{L^5})(CH_3OH)_2]\}_\infty$ (5) and $\{[Ni(\mathbf{L^1})_2(\mathbf{L^5})(CH_3OH)_2]\}_\infty$ (6). Complexes **5** and **6** are isostructural, and here we describe only **5** in detail (see Figure 5 for **5** and Figure S6 and Table S1 for **6** in the Supporting Information). **5** consists of 1D polymeric coordination chains containing only one kind of Co^{II} coordination environment (Figure 5a,b). The asymmetric unit of **5** is composed of one Co^{II}, two $\mathbf{L^1}$ carboxylate groups, one $\mathbf{L^5}$ ligand, and two coordinated CH_3OH molecules. The geometry around each Co^{II} can be best described as a distorted octahedron (Figure 5a). Each Co^{II} is coordinated to two carboxylate O atoms from two different $\mathbf{L^1}$ ligands, another two O atoms from two coordinated CH_3OH molecules, and two N donors from two distinct $\mathbf{L^5}$ ligands. The Co^{II} ion deviates from the least-squares plane generated by O(1)−O(3)−O(1A)−O(3A) toward N(1) by only ca. 0.0176 Å (Table 6).[19] On the other hand, in the coordination environment around each Co^{II}, $\mathbf{L^1}$ adopts a unidentate coordination mode and $\mathbf{L^5}$ serves as a linear bridging ligand [the N(1)···Co(1)···N(2) angle being 180.00°] which links the adjacent Co^{II} ions into a 1D chain (Figure 5b). It should be pointed out that, in the chain structure of **5**, there is intrachain O−H···O H-bonding. The O(3) atoms from CH_3OH not only coordinate to Co^{II} but also act as the H-bonding donors to form O−H···O H-bonding with O(2) of the carboxylate

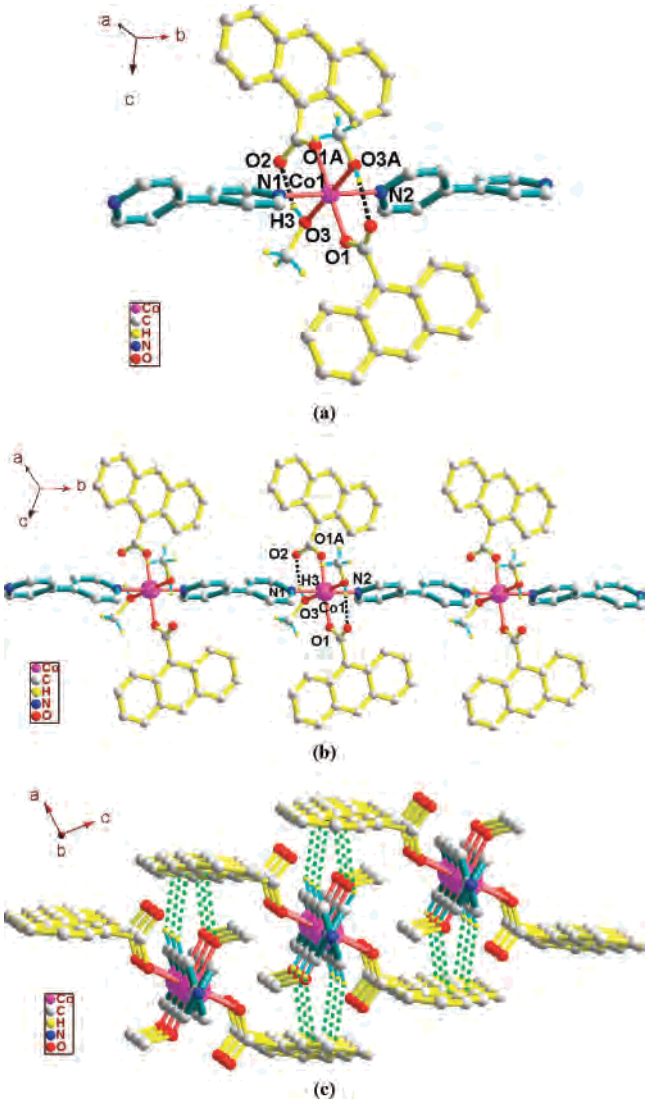

Figure 5. View of (a) the coordination environment of Co^{II} in **5** showing intramolecular O−H···O H-bonding (black dashed lines), (b) the 1D chain showing intrachain O−H···O H-bonding interactions (black dashed lines), and (c) the interchain C−H···π interactions (green dashed lines) in **5** (partial H atoms were omitted for clarity).

Table 6. Selected Bond Distances (Å) and Angles (deg) for Complex **5**[a]

Co(1)−O(1)$^{\#1}$	2.0530(12)	Co(1)−O(1)	2.0530(12)
Co(1)−O(3)	2.1027(13)	Co(1)−O(3)$^{\#1}$	2.1027(13)
Co(1)−N(1)	2.1902(19)	Co(1)−N(2)$^{\#2}$	2.203(2)
O(1)$^{\#1}$−Co(1)−O(1)	177.77(6)	O(1)$^{\#1}$−Co(1)−O(3)	89.57(5)
O(1)−Co(1)−O(3)	90.44(5)	O(1)$^{\#1}$−Co(1)−O(3)$^{\#1}$	90.44(5)
O(1)−Co(1)−O(3)$^{\#1}$	89.57(5)	O(3)−Co(1)−O(3)$^{\#1}$	179.74(6)
O(1)$^{\#1}$−Co(1)−N(1)	91.12(3)	O(1)−Co(1)−N(1)	91.12(3)
O(3)−Co(1)−N(1)	89.87(3)	O(3)$^{\#1}$−Co(1)−N(1)	89.87(3)
O(1)$^{\#1}$−Co(1)−N(2)$^{\#2}$	88.88(3)	O(1)−Co(1)−N(2)$^{\#2}$	88.88(3)
O(3)−Co(1)−N(2)$^{\#2}$	90.13(3)	O(3)$^{\#1}$−Co(1)−N(2)$^{\#2}$	90.13(3)
N(1)−Co(1)−N(2)$^{\#2}$	180.0		

[a] Symmetry codes for **5**: #1, $-x$, y, $-z + 3/2$; #2, x, $y + 1$, z.

groups of the coordinated **L^1** ligands (see also Figure 5a,b and Table 7).[20]

Apart from the obvious interchain $\pi\cdots\pi$ stacking observed here between the anthracene rings of **L^5** (the centroid−centroid and average interplanar separations being 3.566 and 3.3958 Å with a dihedral angle of 0.2°) (see Figure S5 in the Supporting Information), the structure also contains obvious internetwork C−H···π supramolecular interactions between the anthracene and 4,4′-bipyridine rings with an edge-to-face orientation (d = 2.8037 and 3.0432 Å and A = 133.80° and 138.22° in the C−H···π patterns)[21] which link the 1D chain further into a 2D sheet and then a 3D supramolecular network from different crystallographic directions (see Figure 5c).

Table 7. Hydrogen-Bonding Geometry (Å, deg) for **1**, **2**, and **4**−**6**[a]

D−H···A	D−H	H···A	D···A	D−H···A
	1			
O(10)−H(10B)···O(9A)	0.842	2.016	2.851	171.01
C(62)−H(62A)···O(8A)	0.960	2.543	3.401	148.87
	2			
C(62)−H(62A)···O(4A)	0.931	2.546	3.153	122.89
	4			
O(1W)−H(1WA)···O(2)	0.851	1.789	2.626	167.70
O(1W)−H(1WB)···O(3)	0.851	1.750	2.583	165.26
	5			
O(3)−H(3)···O(2)	0.811	1.856	2.632	159.65
	6			
O(3)−H(3A)···O(2A)	0.829	1.843	2.600	151.19

[a] Symmetry codes for **1**: A, x, y, $1 + z$. Symmetry codes for **2**: A, $-x$, $-y + 2$, $-z + 1$. Symmetry codes for **6**: A, $-x + 1$, y, $-z + 3/2$.

Because of the diverse coordination modes and chelating/bridging abilities of the carboxylate groups, new interesting metal−organic frameworks (MOFs) with potential applications often may be achieved by the reactions of carboxylate-containing ligands with various metal salts, especially for aromatic dicarboxylic acids, such as 1,4-benzenedicarboxylic acid and 1,4-naphthalenedicarboxylic acid.[1k,3−7] However, in comparison with such aromatic acids aforementioned, far less common has been the investigation of aromatic anthracene-based dicarboxylic acid in the construction of MOFs, which may be due to the steric hindrance of the bulky anthracene ring skeleton. Following this lead, when we sequentially use 9,10-anthracenedicarboxylic acid (H$_2$**L^6**; see also Chart 1) instead of H**L^1** to react with Cu(NO$_3$)$_2$·4H$_2$O, under the same conditions, a 1D zigzag chain structure is produced.[22] As such, the synthetic procedures described here have also been generally applicable for other metals as well as similar ligands with a bulky aromatic skeleton in our laboratory.[23]

Effect of the Bulky Aromatic Skeleton of the HL^1 Ligand in Self-Assembly of 1−6. As typical aromatic carboxylic ligands, benzene-based and naphthalene-based carboxylic acids, especially their dicarboxylic acids (**BDCA** and **NDCA**; see Chart 1), have been well used to construct metal−organic coordination architectures.[4−7] However, the use of anthracene-based carboxylic acid ligands, such as H**L^1**,

(22) Crystal data for this 1D complex: $C_{26}H_{34}CuN_2O_6$, M = 534.09, monoclinic, space group $P2(1)/c$, a = 11.809(2) Å, b = 10.707(2) Å, c = 20.450(4) Å, β = 105.65(3)°, V = 2490.0(9) Å^3, Z = 4, D_c = 1.425 Mg·m^{-3}, μ(Mo Kα) = 0.921 mm^{-1}, F(000) = 1124, T = 293-(2) K, 18491 reflections measured, 4389 unique reflections (R_{int} = 0.0559), final R1 = 0.0795, wR2 = 0.2004 [for selected data with $I > 2\sigma(I)$], GOF = 1.134 for all data. In addition, H$_2$**L^6** was synthesized according to a reported literature procedure (see: Jones, S.; Atherton, J. C. C.; Elsegood, M. R. J.; Clegg, W. *Acta Crystallogr.* **2000**, C*56*, 881 and references therein).

(23) Liu, C.-S.; Bu, X.-H.; et al. Unpublished results.

an analogue of the relevant benzene-based and naphthalene-based carboxylic acids (H**BA** and H**NCA**; see Chart 1), has not been well-documented to date.[9a,b] From the above descriptions and discussions of crystal structures, it can be seen that H**L**^{1} has two obvious characteristics (see the Introduction) that are different from those of the related benzene- and naphthalene-based carboxylic acids, which often make them show different coordination abilities and modes in the process of constructing metal carboxylate complexes and then form interesting structures.[9a,b] For instance, a 1D Cu^{II}−benzoate complex, [Cu(**BA**)](**BA**)-$(H_2O)_3]_\infty$[8a] (**BA** = $C_6H_5CO_2$, benzoate), and two dinuclear Cu^{II}−benzoate complexes, $[Cu_2(\mathbf{BA})_4(CH_3OH)_2](CH_3OH)$[8b] and $[Cu_2(\mathbf{BA})_4(H\mathbf{BA})_2]$,[8c] have been reported.[8a−c] However, when we use H**L**^{1} instead of H**BA** to react with $Cu(NO_3)_2\cdot 4H_2O$ under certain conditions, only one dinuclear complex, $[Cu_2(\mathbf{L}^{1})_4(CH_3OH)_2](CH_3OH)$ (**1**), is produced. Besides, we have found that two mononuclear Cu^{II}−benzoate complexes incorporating **L**^{2} as an auxiliary chelating ligand, $[Cu(\mathbf{BA})_2(\mathbf{L}^{2})](H_2O)$[8d,e] and $[Cu(\mathbf{BA})(\mathbf{L}^{2})_2](NO_3)(H_2O)$,[8f] are also well documented. In this work, however, the structure of **2** involving **L**^{1} and chelating **L**^{2} provided a tetranuclear motif. As such, we also noticed that two helical coordination polymers with large chiral cavities, $\{[Ni(\mathbf{BA})_2(\mathbf{L}^{5})(CH_3OH)_2](C_6H_5NO_2)_2\}_\infty$ and $\{[Ni(\mathbf{BA})_2(\mathbf{L}^{5})(CH_3OH)_2](CHCl_3)_2\}_\infty$, have been synthesized and reported by M. J. Zaworotko.[8k] The result reveals that chiral crystalline architectures and cavities or channels can be achieved by using the most simple achiral molecular components. In contrast, when we use H**L**^{1} with the bulky skeleton of the aromatic ring to react with $Ni(NO_3)_2\cdot 6H_2O$ incorporating **L**^{5} as an auxiliary bridging ligand, only one 1D achiral coordination polymer (**6**) is produced without any guest molecules included. Thus, although the carboxylic coordination sites of H**L**^{1} and H**BA** are very similar, their coordination chemistries are obviously different presumably due to the skeleton bulk of the anthracene ring.

Our results indicate that the steric bulk of the anthracene ring in H**L**^{1}, by virtue of intra- and/or intermolecular $\pi\cdots\pi$ stacking and C−H$\cdots\pi$ interactions in its complexes, plays an important role in the formation of **1**−**6**, which, from the viewpoint of ligand design, may offer effective means for constructing unique coordination architectures with tailored properties by the steric hindrance of the bulky skeleton.

Magnetic Properties. Variable-temperature and variable-field magnetic susceptibility measurements have been performed on crushed crystalline samples of complexes **1**−**6**. Below, each one will be discussed separately.

The magnetic behavior of **1** is shown in Figure S7 in the Supporting Information. The crystal structure of **1** is analogous to that of copper acetate, with four *syn*−*syn*-carboxylate bridges (see Figure 1a). Such a structural motif leads to a very short Cu−Cu distance of only 2.608 Å, which allows for the direct overlap of the magnetic orbitals. This is reflected in large J values that can be as large as −300 cm^{-1}.[24−25] Theoretical analysis of this kind of dinuclear *syn*−*syn*-carboxylato-bridged Cu^{II} complexes was recently reported.[25] As expected from the crystal structure, the magnetic behavior of **1** is analogous to that of copper acetate; therefore, **1** displays very strong antiferromagnetic coupling between the two Cu^{II} ions. $\chi_M T$ measured at an applied dc field of 1.0 T has a value of less than 0.2 cm^3 K mol^{-1} at room temperature (see Figure S7b in the Supporting Information), indicating very strong antiferromagnetic coupling between the Cu^{II} ions. As the temperature decreases to 2 K, $\chi_M T$ decreases until it reaches a value of 0. Magnetization vs field measurements at 2 K in the 500−50000 G field range remain below 0.010, supporting the $S = 0$ spin ground state (see Figure S7a in the Supporting Information).

Complex **3** also contains the paddle-wheel dinuclear Cu−Cu unit with four carboxylates (see Figure 3). In fact, the $\chi_M T$ value at 300 K was measured, and its magnetic behavior is analogous to that of **1**. Further measurements on **3** were not pursued in detail.

The magnetic susceptibility for **2** was measured at 1.0 T (see Figure 6a). $\chi_M T$ at 300 K has a value of 1.78 cm^3 K mol^{-1}, slightly higher than the 1.5 cm^3 K mol^{-1} expected for four noninteracting Cu^{II} ions. It remains nearly constant down to 50 K; at this temperature, a sharp drop in $\chi_M T$ is observed. The $\chi_M T$ value at 2 K is 0.23 cm^3 K mol^{-1}. This complex will be considered as a dimer of dimers for the interpretation of the magnetic behavior. Each of these dimers contains two Cu^{II} ions [Cu(1), Cu(2) and Cu(1A), Cu(2A)] and the corresponding ligands. The dimers are linked as follows (see Figure 2a): Cu(1) is linked to Cu(2A) and Cu-(2) is linked to Cu(1A) by single *syn*−*anti*-carboxylate bridges [O5, O(6A) and O(5A), O(6)]. Cu(1) and Cu(2) are 3.287(4) Å apart, bridged by two O atoms [O(3) and O(6)] from two different carboxylates and by a third carboxylate in the common *syn*−*syn* bridging mode. Cu(1) is in a distorted octahedral environment, with an elongation along the Cu(1)$\cdots$O(3) nonbonding contact [the Cu(1)$\cdots$O(3) separation being 2.492 Å]. Cu(2) is pentacoordinated in a square-pyramidal fashion, and the Cu(2)−O(6) bond distance of 2.302(3) Å is located in the apical position of the pyramid. The coupling through these two monatomic bridges is expected to be very weak, since in both cases the $d_{x^2-y^2}$ orbital of one Cu^{II} interacts with the d_{z^2} orbital of the other Cu^{II} ion. The main pathway for exchange is then through the *syn*−*syn*-carboxylate. The data obtained were fit using the computer program CLUMAG,[26] which uses the irreducible tensor operator formalism. With the spin Hamiltonian $\hat{H} = -J_1(\hat{S}_1\cdot\hat{S}_2 + \hat{S}_2\cdot\hat{S}_3) - J_2(\hat{S}_2\cdot\hat{S}_3)$ and the atom labeling as in Scheme 2, the best agreement obtained was for $J_1 = -4.82$ cm^{-1}, $J_2 = |1.28|$ cm^{-1}, and $g = 2.23$. The fit shown in Figure 6a as a solid line corresponds to $J_2 = -1.28$ cm^{-1},

(24) (a) Dalai, S.; Mukherjee, P. S.; Zangrando, E.; Lloret, F.; Chaudhuri, N. R. *J. Chem. Soc., Dalton Trans*. **2002**, 822 and references therein. (b) Muto, Y.; Nakashima, M.; Tokii, T.; Suzuki, I.; Ohba, S.; Steward, O. W.; Kato, M. *Bull. Chem. Soc. Jpn.* **2002**, *75*, 511 and references therein. (c) Steward, O. W.; McAfee, R. C.; Chang, S. C.; Piskor, S. R.; Schreiber, W. J.; Jury, C. F.; Taylor, C. E.; Pletcher, J. F.; Chen, C. S. *Inorg. Chem.* **1986**, *25*, 771. (d) Kahn, O. *Molecular Magnetism*; VCH: New York, 1993.
(25) Rodríguez-Fortea, A.; Alemany, P.; Alvarez, S.; Ruiz, E. *Chem.*−*Eur. J.* **2001**, *7*, 627.
(26) Gatteschi, D.; Pardi, L. *Gazz. Chim. Ital.* **1993**, *123*, 231.

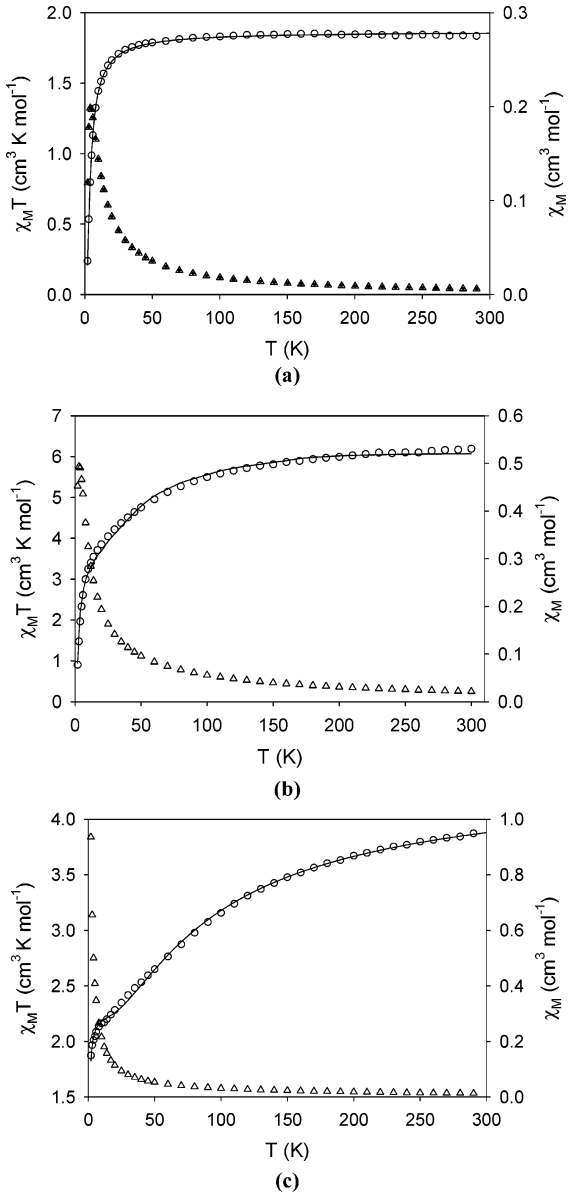

Figure 6. (a) $\chi_M T$ vs T (○) and χ_M vs T (△) for **2**, (b)$\chi_M T$ vs T (○) and χ_M vs T (△) for **4**, and (c) $\chi_M T$ vs T (○) and χ_M vs T (△) for **5** (the solid lines are the best fits to the experimental data).

Scheme 2. Atom Labeling Scheme of **2** for Related Analysis of the Magnetic Properties

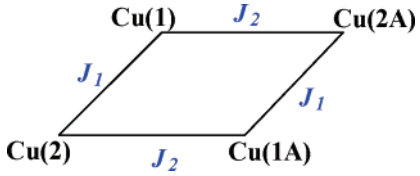

but just as good a calculated curve is obtained for $J_2 = +1.28$ cm^{-1}. The J values can be rationalized on the basis of the structural features of **2**. As Ruiz et al. showed,[25] the exchange constants of two Cu^{II} ions bridged by a single *syn*−*syn*-carboxylate are on the order of 3 cm^{-1}, and accordingly, the calculated value of J_1 is −4.93 cm^{-1}. Therefore, **2** can be described as two $S = 0$ Cu_2 units bridged by *syn*−*anti*-carboxylate bridges. As calculated by Ruiz et al.,[25] the exchange interaction between two Cu^{II} ions through a single *syn*−*anti*-carboxylate is very weak and can be either antiferromagnetic or ferromagnetic. In this situation, the antiferromagnetic value of J_1 will dominate the magnetic behavior, and it is very difficult to accurately determine the value and sign of J_2. Magnetization vs field data of **2** were collected at 2 K in the 500−50000 G field range (see Figure S8 in the Supporting Information). The increase of the magnetization with increasing field is due to the Boltzmann population of excited states that possess an S value larger than the $S = 0$ ground state and are thus split by the external field.

The magnetic susceptibility for **4** was measured in an applied dc field of 0.5 T (see Figure 6b). At 300 K, the $\chi_M T$ value for **4** was 3.5 cm^3 K mol^{-1}. This is in agreement with having two high-spin Co^{II} ions with strong spin−orbit coupling. As temperature decreases, $\chi_M T$ also decreases, indicating the presence of antiferromagnetic coupling between the metal centers. A sharp drop is observed below 25 K, the value at 2 K being 0.9 cm^3 K mol^{-1}, indicating the depopulation of the excited states. For many years, the only available theory to quantitatively study the exchange coupling in dinuclear and trinuclear Co^{II} complexes has been that proposed by Lines.[27] In this theory, a perfect octahedral high-spin Co^{II} complex is assumed. Unfortunately, Co^{II} centers usually display a strong distortion with regard to the perfect octahedral geometry. Recently, Lloret[28] and Cano[29] have revisited this problem in dinuclear Co^{II} systems assuming axial distortion. In this case, the triplet orbital $^4T_{1g}$ ground state splits into a singlet $^4A_2$ level and a doublet ^4E level with a D energy gap. The one-center operator responsible for axial distortion is expressed by

$$M_{ax} = D[L_z^2 - (1/3)L(L+1)]$$

The Hamiltonian involving the magnetic exchange, spin−orbit coupling, axial distortion, and Zeeman interaction is given by eq 1. In the weak crystal field limit ($B \gg Dq$), A

$$H = -JS_1S_2 - A\kappa\lambda LS + D[L_z^2 - (1/3)L(L+1)] + \mu_B(-A\kappa L + g_eS)H \quad (1)$$

$= 1.5$, whereas in the strong crystal field limit ($B \ll Dq$), $A = 1$. As was indicated by Lloret and Cano, no analytical expression for the magnetic susceptibility as a function of J, A, κ, λ, and D can be derived. The values of these parameters have to be determined through numerical matrix diagonalization. The VPMAG package developed by Cano[29] has been used to fit the experimental data. The experimental curve for two Co^{II} ions and the best fit are shown in Figure 6. The best fit values were $A\kappa = 1.26$, $D = 143$ cm^{-1}, $\lambda = -138$ cm^{-1} (λ for the free ion is −175 cm^{-1}), and $J = -1.58$ cm^{-1} with $F = 2.5 \times 10^{-4}$ (F is the agreement factor defined as $\sum(\chi_m T_{exptl} - \chi_m T_{theor})^2)/\sum(\chi_m T_{exptl})^2$. The value obtained

(27) (a) Lines, M. E. *J. Chem. Phys.* **1971**, *55*, 2977. (b) Munno, G. De; Julve, M.; Lloret, F.; Faus, J.; Caneschi, A. *J. Chem. Soc., Dalton Trans.* **1994**, 1175.
(28) Mishra, V.; Lloret, F.; Mukherjee, R. *Inorg. Chim. Acta* **2006**, *359*, 4053.
(29) Cano, J. *VPMAG package*, B.1 revision; University of Valencia: Valencia, Spain, 2003.

for J(Co−Co) indicates weak antiferromagnetic exchange, which is what is expected for two Co^{II} centers with competing magnetic interactions. The two *syn*−*syn*-carboxylates will mediate antiferromagnetic exchange, while a Co−O−Co bridge (O from H_2O) with an angle of 117° could lead to weak ferromagnetic coupling. Overall the antiferromagnetic interaction is stronger and the dimer is antiferromagnetically coupled.

The variable-field magnetization data for **5** were collected in the 500−50000 G field range (see Figure S9 in the Supporting Information). The data are typical for a Co^{II} ion with strong spin−orbit coupling.[30] Variable-temperature data were collected at an applied dc field of 5000 G in the 2−300 K temperature range (see Figure 6c). $\chi_M T$ at 300 K is 3.89 cm^3 K mol^{-1} ($S = 3/2$). As temperature decreases, the $\chi_M T$ value also decreases, following the Curie−Weiss law until 50 K. The exchange interaction seems to be weak, and a phenomenological approach was taken to estimate the exchange constant between the Co^{II} centers. This has been shown to give good results by Rabu and co-workers.[31] The only possible exchange pathways between the Co^{II} ions in the 1D chains of **5** are the $\mathbf{L^5}$ ligands and the $\pi\cdots\pi$ stacking of the anthracene aromatic groups of the carboxylates (~4.0 Å apart); both of these will only mediate a very weak coupling, the model only allows for one exchange parameter, and all of the interactions are grouped in the exchange constant calculated, J. Equation 2 has been used to fit the

$$\chi T = A \exp(-E_1/kT) + B \exp(-E_2/kT) \qquad (2)$$

experimental data, and the best fit is shown in Figure 6c as a solid line. In eq 2, $A + B$ equals the Curie constant and E_1 and E_2 represent "activation energies" corresponding to the spin−orbit coupling and the antiferromagnetic interaction. The equation describes well the effect of the spin−orbit coupling, which causes exponential low-temperature divergence of the susceptibility. The obtained values are $A + B = 4.40$, $E_1 = 59.19$ cm^{-1}, and $-E_2 = -0.30$ cm^{-1}. The $A + B$ value is consistent with the Curie constant calculated from the high-temperature data, and E_1 is in good agreement with the expected values for the spin−orbit coupling as reported by Rabu et al.[31] (E_1 has values on the order of 70 cm^{-1}). As for the antiferromagnetic exchange, it is very weak indeed, corresponding to $J = -0.60$ cm^{-1} according to the Ising chain approximation.

The variable-temperature magnetic susceptibility data were collected for **6** at an applied dc field of 0.7 T in the 2−300 K temperature range (see Figure S10a in the Supporting Information). The $\chi_M T$ product remains nearly constant in the entire temperature range at a value of 1.1 cm^3 K mol^{-1}, as expected for isolated Ni^{II} ions with $S = 1$. This is in agreement with the lack of suitable magnetic exchange pathways between the metal centers in the solid. Variable-field magnetization measurements at 2 K support this statement (see Figure S10b in the Supporting Information), as the reduced magnetization curve for **6** overlaps with the Brillouin function for an $S = 1$ ion.

XRPD Results. To confirm whether the crystal structures are truly representative of the bulk materials, XRPD experiments have been carried out for **1**−**6**. The XRPD experimental and computer-simulated patterns of the corresponding complexes are shown in Figure S11 in the Supporting Information. Although the experimental patterns have a few unindexed diffraction lines and some are slightly broadened in comparison with those simulated from the single-crystal modes, it still can be considered favorable that the bulk synthesized materials and the as-grown crystals are homogeneous for **1**−**6**.

Concluding Remarks

We have successfully obtained a series of new Cu^{II}, Co^{II}, and Ni^{II} complexes having dinuclear, tetranuclear, and 1D structures with the bulky anthracene-based carboxylic ligand H$\mathbf{L^1}$, sometimes incorporating different auxiliary ligands (chelating or bridging). The results reveal that, in comparison with structurally related benzene- or naphthalene-based carboxylic acids, the bulky anthracene skeleton of H$\mathbf{L^1}$, by virtue of intra- and/or intermolecular $\pi\cdots\pi$ stacking and C−H$\cdots\pi$ interactions in their complexes plays an important role in the formation of **1**−**6**. Moreover, the magnetic properties for **1**−**6** have been investigated and discussed in detail, along with the corresponding J parameter related to their structural characteristics. In complexes **1** and **3** the very short Cu−Cu distance typical of the paddle-wheel structure of copper acetate results in strong antiferromagnetic coupling. In **2** and **4**−**6** the coupling between the metal centers is weak, due to the long M−M separation imposed by the bulky ligands. Finally, the procedures described here might be generally applicable for the analogous bulky aromatic carboxylic ligands and different metal ions (especially for mixed-metal systems such as Zn−Ln, Cd−Ln, and Mn−Ln) in the aspect of constructing other metal−organic complexes.

Acknowledgment. This work was supported by the Natural Science Foundation of China (Grant Nos. 20531040 and 50673043) and the Spanish government (Grant CTQ2006/03949/BQU and Juan de la Cierva Fellowship to E.C.S.). We thank Prof. Huai-Lin Sun and Ms. Jiang-Yu Zhao of the Department of Chemistry, Nankai University, for technical assistance.

Supporting Information Available: Crystallographic information files (CIFs) of complexes **1**−**6**, additional figures for complexes **1**−**6** (Figures S1−S6), additional table for complex **6** (Table S1), additional plots of the susceptibility and magnetization data for the various complexes (Figures S7−S10), and XPRD patterns for all complexes (Figure S11). This material is available free of charge via the Internet at http://pubs.acs.org.

IC070086Y

(30) Carlin, R. L. *Magnetochemistry*; Springer-Verlag: New York, 1986.
(31) Rueff, J. M.; Masciocchi, N.; Rabu, P.; Sironi, A.; Skolius, A. *Chem.*−*Eur. J.* **2002**, *8*, 1813.